Tooling-integrated sensing systems for stamping process monitoring

Numpon Mahayotsanun [a], Sripati Sah [b], Jian Cao [a,*], Michael Peshkin [a], Robert X. Gao [b], Chuan-tao Wang [c]

[a] Department of Mechanical Engineering, Northwestern University, Evanston, IL 60208, USA
[b] Department of Mechanical Engineering, University of Connecticut, Storrs, CT 06269, USA
[c] Body Manufacturing Engineering, General Motors Corporation, Warren, MI 48090, USA

ARTICLE INFO

ABSTRACT

In-situ stamping process monitoring plays a critical role in enhancing productivity and ensuring part quality in sheet metal stamping. This paper investigates the realization of two sensing methods to create a tooling-integrated sensing system: mutual inductance-based displacement measurement for sheet draw-in, and distributed contact pressure measurement at the tool–workpiece interface. The two sensing systems are complementary in nature, and together, they significantly enhance the on-line observability of the stamping process. The performance of the draw-in sensor was evaluated using numerical simulations and experiments in a small-scale and a large-scale lab setup, and its effectiveness has been confirmed under the presence of wrinkled sheet. To study the spatial and temporal variations of the tool–workpiece contact pressure in a stamping operation, experiments were conducted on a customized panel stamping test-bed with an array of thin-film force sensors embedded below the die flange and die cavity. The force sensor data were then numerically interpolated to form the contact pressure distribution across the tool–workpiece interface, based on the thin plate spline (TPS) method. Comparison between the interpolated pressure obtained from the surface generation techniques and direct measurement using redundant sensors and a press mounted load cell confirms the validity of the new contact pressure sensing method. The integrated sensing technique provides insight into the stamping process by quantifying process variations and providing a reference base for process control to reduce product disparities. Additionally, new product and process designs can be created based on the quantified and referenced variations.

Published by Elsevier Ltd.

1. Introduction

Due to the inherent high speed associated with the stamping operation, design flexibility, and the ability to work harden material, sheet metal stamping has been widely adopted for making industrial as well as commercial products, such as panels for automobiles, aircrafts, ships, and beverage cans.

The physical setup of a stamping operation (Fig. 1) consists of three main components: the die, the binder, and the punch. In a stamping operation, the punch moves down pressing the work-piece into the die causing plastic deformation of the workpiece material. The binder force regulates the flow of the workpiece into the die cavity by clamping the workpiece periphery between the binder and the die flange during the forming process. The movement of the workpiece edge between the binder and the die flange is known as drawn-in. The draw-in amount is an

important manufacturing index in sheet metal forming and is an indicator of the success of a forming process [1,2]. Insufficient draw-in causes splits and excessive thinning in stamped parts while excessive draw-in induces wrinkles and surface defects on the manufactured parts. Existing draw-in sensors include the LVDT type (Fig. 2 [3]) and the mouse type (Fig. 3 [4]). The LVDT-type draw-in sensor is based on the resistance and requires a physical touch of the tip on the sheet metal edge. The contact between the sheet and the LVDT tip could be lost when the edge starts to wrinkle. The mouse-type draw-in sensor is based on the rotary contact between the sheet metal and the ball embedded in the die surface. It also requires a physical contact between the sheet and the ball installed in the tooling, which will inevitably introduce wear and alter the measurement result without warning. In order to continuously and reliably measure the draw-in amount of sheet metals in a stamping process without interference with continuous stamping operation, the draw-in sensor based on mutual inductance was developed. The results can be used to quantify process variations in sheet metal stamping and provide a reference base for process control to

* Corresponding author.
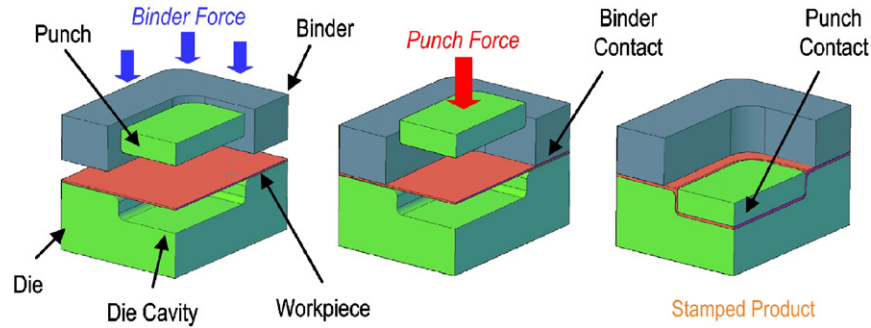E-mail address: jcao@northwestern.edu (J. Cao).

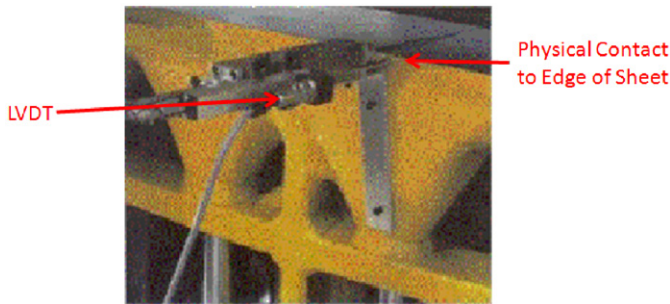**Fig. 1.** Physical setup of stamping operation.

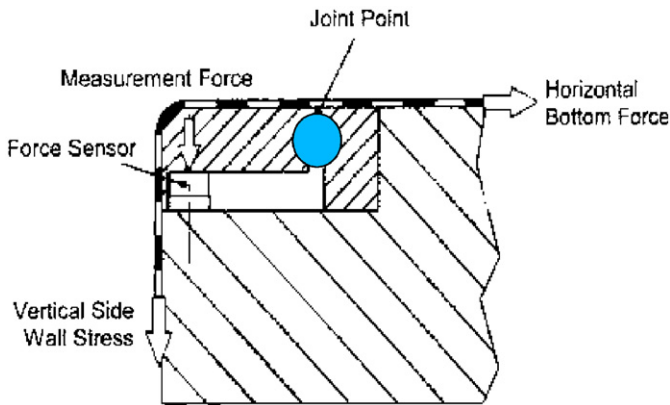

Fig. 2. LVDT-type draw-in sensor.

Fig. 3. Mouse-type draw-in sensor.

reduce product disparities. Additionally, new product and process designs can be created based on the quantified and referenced variations.

Previous research has established that concurrent to workpiece draw-in characteristics, the variations in tool–workpiece contact pressure distribution are a critical contributing factor in the occurrence and severity of forming defects [5,6]. The causal relationship between tool–workpiece contact pressure distribution and defect formation provides the basis for a new sensing method for monitoring the stamping process, leading to the idea that forming defects are concomitant with variations in the pressure distribution across the tool–workpiece interface, and that on-line measurement of the contact pressure will allow advances in stamping process monitoring and control. Research in embedded sensing for sheet metal-forming processes monitoring was initiated in the 1990s [7–9], and the primary focus was on development of sensors capable of tool integration. The research

looked at the effect of sensor-tool integration on measurement sensitivity. The exploratory work opened up new possibilities for in-process monitoring. In the intervening years, much progress has been made in sensor packaging and a wide variety of piezoresistive and piezoelectric force sensors that are of low cost, high resolution, and small foot-print became commercially available. This stimulates new research activities that aim at extracting contact pressure distribution across the workpiece–tooling interface by means of an array of embedded force sensors, for improved observability and controllability in sheet metal stamping. Through correlation of multi-physical parameters, e.g. contact pressure, draw-in punch force, and press travel in describing a single forming event, new venues for research in data fusion and process modeling can be initiated.

It is known that variations in a stamping operation can lead to local variations in the pressure distribution over the work piece, such as die wear, die misalignment, wrinkling, thinning, material properties, lubrication, or punch travel [10,11]. A direct approach to interpreting the dynamic pressure distribution on the tool–workpiece interface is through a time indexed series of three-dimensional surfaces, each surface representing the contact pressure distribution at a time instant. This method requires the generation of three-dimensional surfaces that are numerically interpolated from discrete sensor measurements. In the present work, thin plate splines (TPSs) are investigated for estimating the forming pressure distributions from force sensors embedded in a stamping test-bed. By combining the TPS surfaces with process analysis tools, the contact pressure information can be utilized for improved process monitoring and die design (Fig. 4). Furthermore, a tooling-integrated distributed sensing system can enhance condition-based maintenance by providing information to address localized tool wear [12].

The remainder of this paper is organized into two sections. The first section describes the draw-in sensor and the testing results, and the second section introduces the evaluation of thin plate splines for interpolating the forming pressure distribution on a lab-scale stamping tool from an array of spatially distributed sensors. Finally, conclusion from the research findings are drawn, and future work are presented.

2. Draw-in sensing

2.1. Sensing principle

Based on the principle of mutual inductance [13,14], a draw-in sensor was developed. As shown in Fig. 5, the excitation current (i) flowing in the primary coil induces electromotive force (emf) in the secondary coil. The presence of metal (ferrous or non-ferrous) near the coils affects the magnetic field lines, displayed on the right-hand side of Fig. 5, changing the degree of mutual inductance.
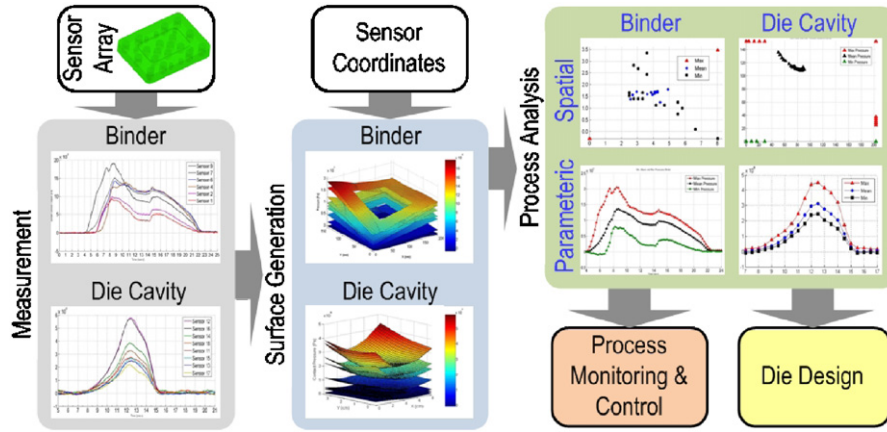
Fig. 4. Embedded sensing for stamping process monitoring and die design.
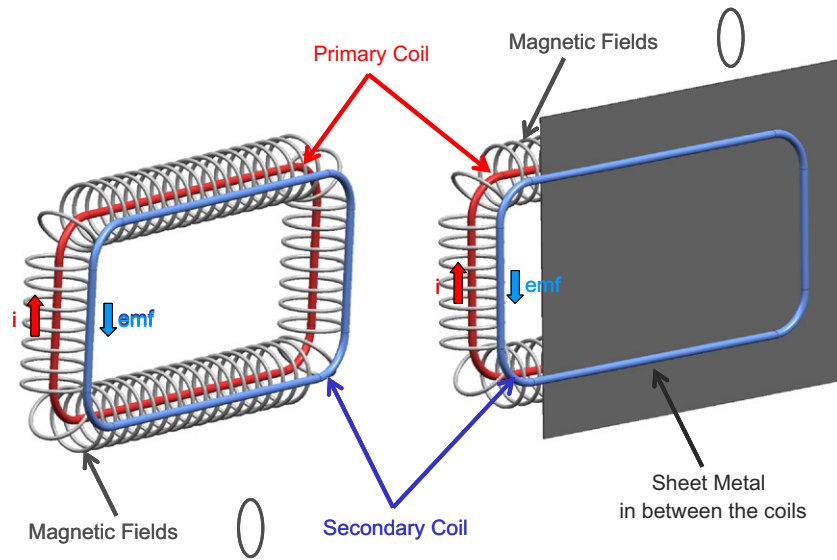

Fig. 5. Draw-in sensor principle.

Thus, the induced signals in the secondary coil reflect how much of the coil is covered up. The difference in the obtained induced signals reflects the different amount of the coil being covered by the sheet metal. Therefore, if one has a sheet partially covering the coils initially and then being pulled to a different position, the sensor will be able to detect the difference of induced *emf* and that difference can be covered to the draw-in amount that of interest.

The induced voltages can be calculated based on the schematic shown in Fig. 6 and the equations as follow. Note that this analytical model did not include the electromagnetic properties of the materials for simplicity. Using the Biot–Savart law, the magnetic fields (B) in the secondary coil can be represented as

$$B = \left(\frac{2N_1 l w \mu_0 i}{4\pi}\right) \left[\frac{1}{((w^2/4) + k^2)^{3/2}} + \frac{1}{((l^2/4) + k^2)^{3/2}}\right] \quad (1)$$

where N_1 is the number of primary coils, l the transducer length of the uncovered zone, w the transducer width, μ_0 the permeability constant of air, i the excitation current (20 mA in our setup), and k the gap distance between the two coils. Then, the magnetic flux through the secondary coil can be obtained as follows:

$$\Phi_B = \int \vec{B} \bullet d\vec{A}_{abcd} \quad (2)$$

where Φ_B is the magnetic flux and $\vec{A}_{abcd}$ the area of the secondary coil. Finally, by using Faraday's law, the induced *emf* in the secondary coil is found as follows:

$$\varepsilon = \frac{-N_1 N_2 l^2 w^2 \mu_0 i_0 f \; \cos(2\pi ft)}{2} \left[\frac{1}{((w^2/4) + k^2)^{3/2}} + \frac{1}{((l^2/4) + k^2)^{3/2}}\right] \quad (3)$$

where ε is the induced *emf*, f the excitation frequency (64 KHz), and t the time.

Based on the above sensing principle, a draw-in sensor was designed which consists of two main components: two transducers (primary and secondary coils) and a data acquisition board. The design of the transducer is shown in Fig. 7 (top), with its physical implementation consisting of a silicon trace embedded in a prototype circuit board (middle). This design makes it possible to readily insert the sensor module into a die slot as shown in the bottom image of Fig. 7. The surface of the transducer was covered with a thin layer of epoxy (0.76 mm in the present study) to prevent scratch from the sliding sheet metal. The data acquisition board provides the excitation current to the primary transducer, receives the induced voltages from the secondary transducer, conducts signal processing and sends the amplified voltage readings to the computer. Since the draw-in sensor is based on the electromagnetic
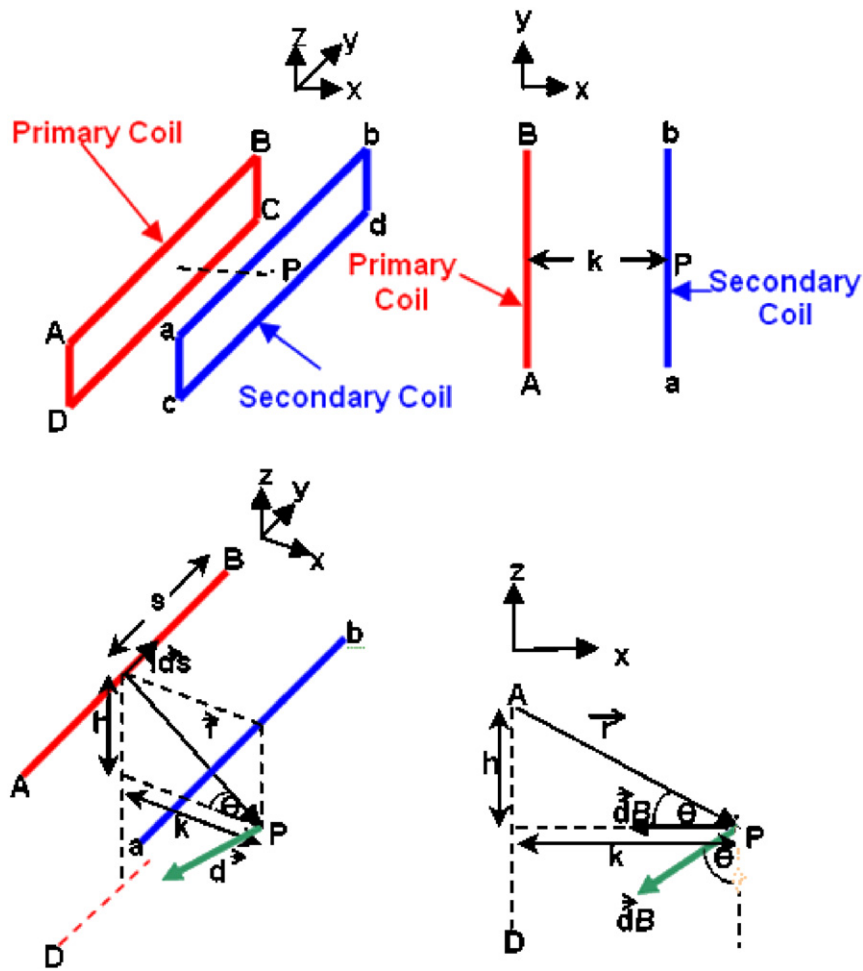
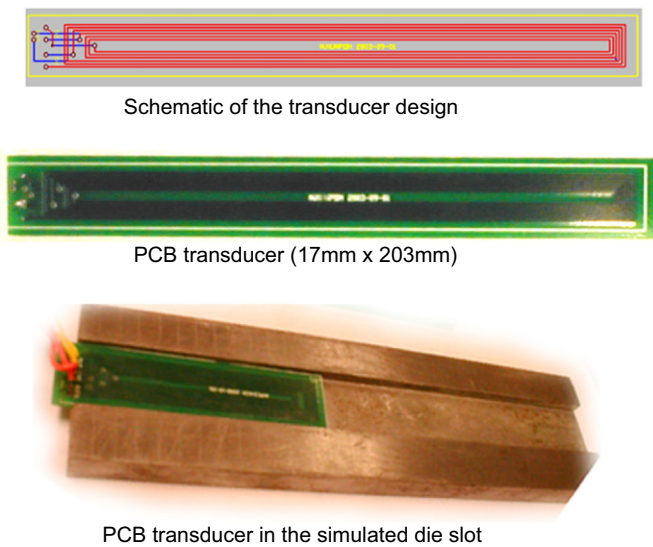**Fig. 6.** Draw-in sensor schematic for induced voltages calculation.

Schematic of the transducer design

PCB transducer (17mm x 203mm)

PCB transducer in the simulated die slot

Fig. 7. Draw-in sensor transducers.

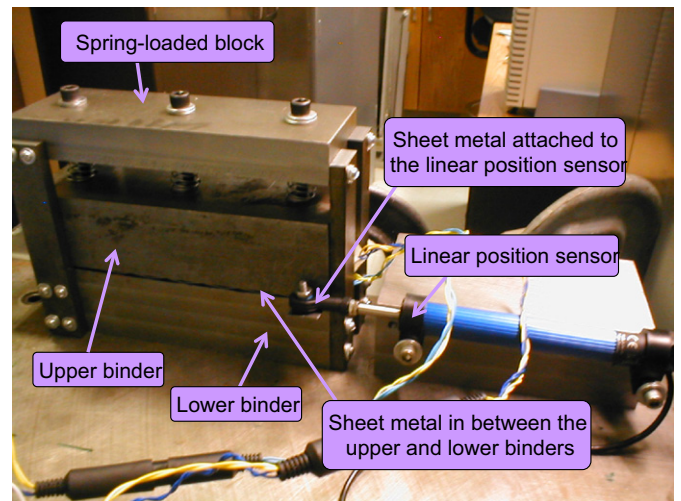**Fig. 8.** Simulated binder pair setup with draw-in sensors embedded in the lower and/or upper binder and a sheet metal in between the binders.

field and the field response is mainly from the two transducers, the induced voltages are continuous and the hysteresis is negligible. The resolution of the sensor is then based on the resolution of the A/D converter. In our application, the A/D converter is a 16-bit one, which converts to a resolution of 7.5×10^{-4} mm.

A lab-scale (20 cm long) stamping simulator was constructed as shown in Fig. 8. The primary transducer was inserted in the lower binder and the secondary transducer was located in the upper binder. A sheet metal was placed in between and fully covered the two transducers at the initial stage. During the experiment, the sheet metal was pulled out of the transducers,

changing the magnetic coupling area and the induced voltages. The induced voltage signals were then recorded with the pulling distance of the sheet. To calibrate this new draw-in sensor and to verify its result, the tip of the linear position sensor (LVDT sensor) was attached to the sheet metal to provide the reference data. Four major factors influencing the characteristics of the draw-in sensor were considered: (1) sheet materials, (2) transducer widths, (3) gap distance between the transducer and the sheet metal, and (4) material flatness.

In order to determine its feasibility and functionality, the draw-in sensors were installed in a 1 m × 1 m die and tested in a 150-t hydraulic stamping press (Fig. 9). The upper and lower binders of a door-shaped die were machined to create slots for embedding the transducers and the material used in the stamping tests was 1.56 mm-thick aluminum alloy Al5182. In each stamping test, the sheet was placed in between the upper and lower binders, and the punch was set to move down, deforming the sheet, at different drawing positions as illustrated in Fig. 10. During the entire stamping test, the transducers detected the movement of the sheet and transmitted the changing induced

voltages to the data acquisition board. The punch displacement was recorded by a displacement sensor mounted on the hydraulic press and later mapped with the draw-in amounts obtained from the draw-in sensor to obtain continuous real-time draw-in histories at those six locations.

The draw-in amounts measured by the sensors in the stamping process were compared with those obtained from using a caliper that measured the draw-in amounts at six locations after each stamping step. The drawback of using caliper, in addition to the time-consuming nature of such a manual measurement method, was its inability to capture the entire draw-in histories, as only discrete draw-in amounts were obtained from the manual measurements.

2.2. Draw-in sensor results

Fig. 11 shows the recorded voltage from the draw-in sensor versus the displacement obtained from the LVDT sensor in the lab-scale setup in Fig. 8. The repeatability of the measurement result
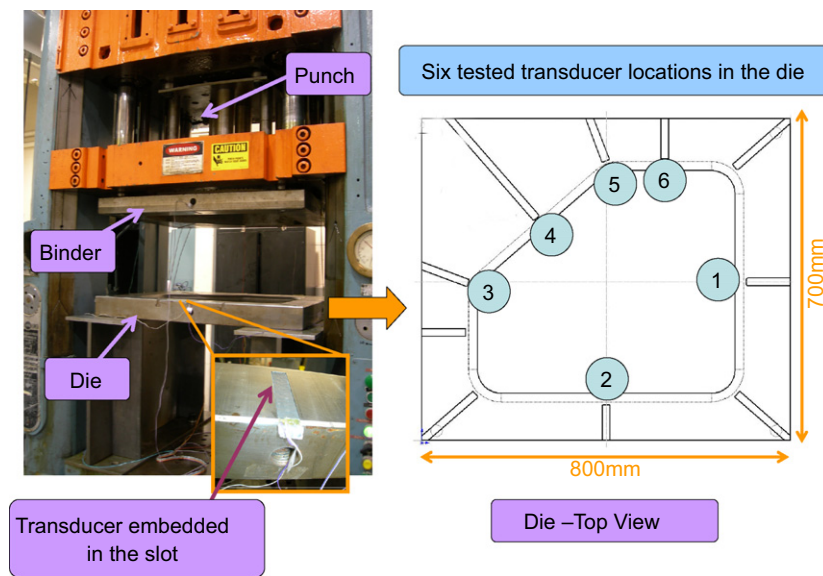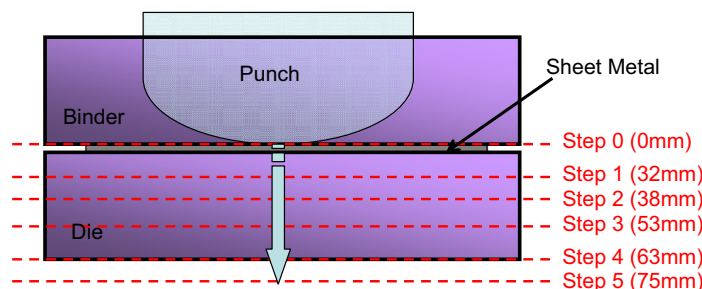

Fig. 9. Locations of draw-in transducers mounted in a stamping die set.
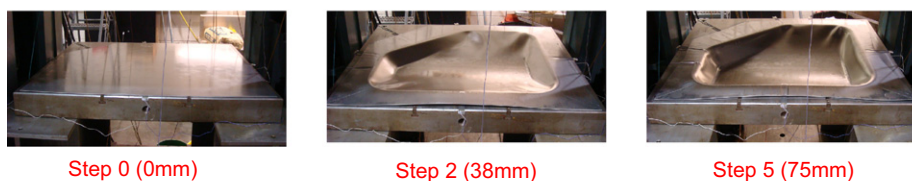

Fig. 10. Stamping steps.

is seen in Fig. 11, which is based on five tests. As the figure shows, a near linear relationship exists between the draw-in displacement and the recorded induced voltage. This relationship can be characterized by the slope of the displacement–voltage curve. The effect of the four factors considered in the present study can be summarized as follows:

(1) Different materials lead to different slopes due to the differences in the electromagnetic properties of each material.
(2) Wider transducers provide higher induced voltages because of the increase in the magnetic coupling area.
(3) The strength of the magnetic coupling area decreases (induced voltages decrease) linearly with an increasing gap between the transducers.
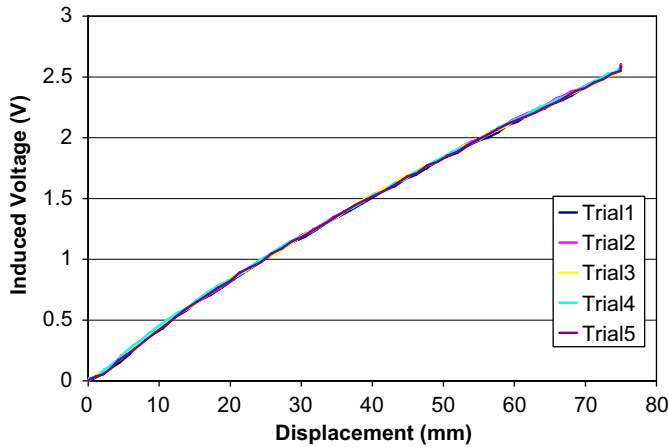(4) The draw-in sensor is insensitive to material shape when the sheet thickness is thinner than approximately 1 mm.

One of the major questions to be addressed from this lab-scale setup is whether the draw-in amount can be measured under the presence of a wrinkled sheet. Fig. 12 shows the capability of the sensor. Although there appears a slight difference between the experimental and simulation results due to the gap changes caused by sheet pulling, the sensor was found to be insensitive to the flatness of the sheet from both simulations and experimental results, which is desirable in the draw-in measurement.
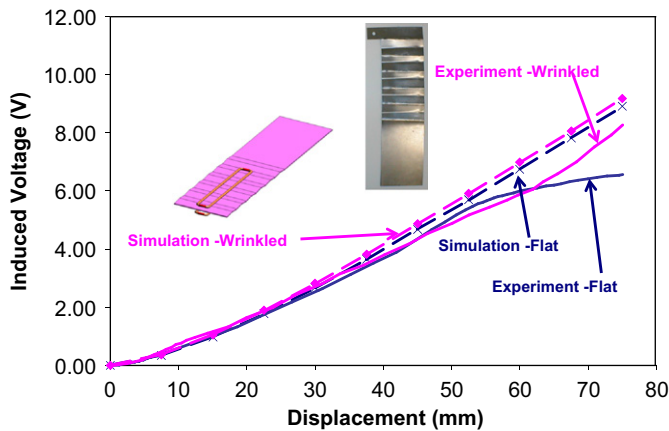
In addition to the experimental results, analytical and simulation models of the draw-in sensor were constructed to verify the validity of the experimental results. The analytical model was created based on Eqs. (1)–(3). The slopes of the induced voltages with respect to the sheet displacement from each case are plotted against the sheet thickness in Fig. 13. The difference between the experimental results and those of the analytical and simulation was mainly due to the gap distances between the transducers in the experiments, as a theoretically zero gap was considered in the models. Nevertheless, the results of all three methods were found to be in good agreement. This confirms that the numerical model can be used to anticipate the expected slope, once a new design or a new material is in place.

The results from the industry-scale draw-in sensor and manual measurements using a caliper are shown in Fig. 14. One test sheet was used from steps 1 to 5 where punch displacements were different. At the end of each step, sheet metal would spring back, thus, resulting in the discontinuity observed from the draw-in sensors. The plot presents the combined draw-in sensor results of all five stamping steps versus the punch displacement. As can be seen from Fig. 14, the two methods provided similar results at all six draw-in locations while the draw-in sensors provided continuous draw-in histories.

Fig. 11. Repeatability results of lab-scale setup test using 12.7 mm wide transducers with flat 1.66 mm thick aluminum Al 5052 sheet and an embedded depth of 3.32 mm.

Fig. 12. Experimental and simulation results of testing flat and wrinkled 0.64 mm steel 1018 sheets using the 12.7 mm wide transducers at 0 t gap.
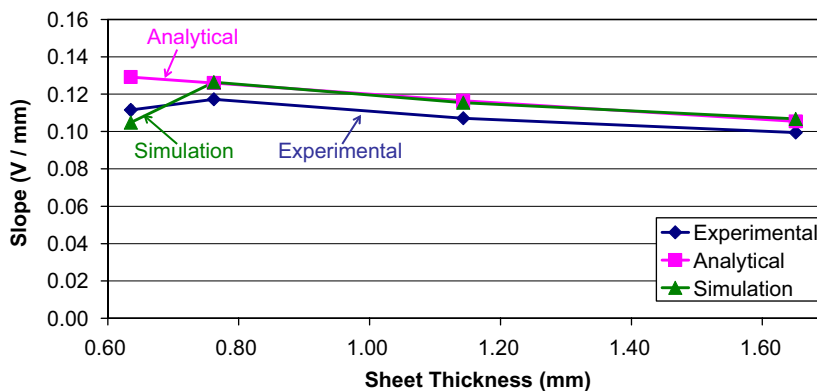

Fig. 13. Comparison among the experimental, analytical and simulation methods of the tests using 12.7 mm wide draw-in transducers.
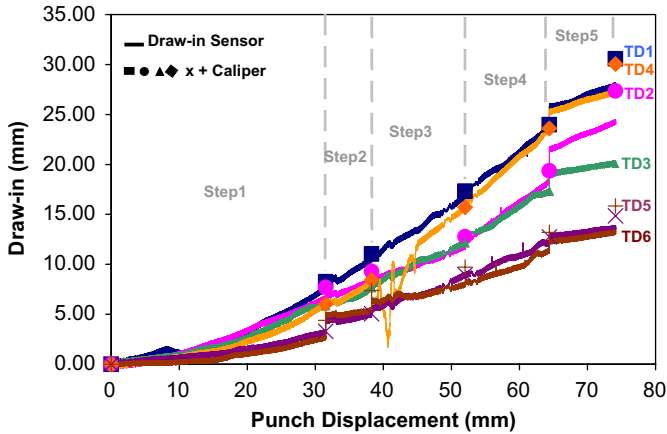
Fig. 14. Draw-in results comparison between the draw-in sensor and caliper measurements of forming 1.56 mm thick aluminum Al5182 at different punch displacements.

Table 1
Specifications of sensors used in experiments.

	Specifications
Linearity error	$< \pm 3\%$
Repeatability error	$< \pm 2.5\%$ Full scale
Hysteresis error	$< 4.5\%$ Full scale
Response time	$< 5\,\mu s$
Drift (steady input)	$< 5\%$ Per logarithmic time

3. Embedded pressure sensing

The contact pressure on the tool–workpiece interface was derived from data measured by commercially available piezo-resistive thin-film force sensors. A sensor cap was placed on the top of the thin-film sensor where stamping force is transmitted. Technical specifications of the force sensor supplied by the manufacturer are shown in Table 1. Given that embedding sensors into the die structure affects the structural integrity of the die, it is essential to minimize the number of sensors to be embedded while ensuring an accurate reconstruction of contact pressure distribution on the tooling–workpiece interface. In the present study, this goal is achieved with the assistance of the thin plate spline numerical surface interpolation technique. This technique was utilized to recreate spatially continuous pressure profiles based on measurements from spatially distributed force sensors. The accuracy of the TPS-based interpolation has been experimentally verified through evaluation of the contact pressure distribution on the tool–workpiece contact interface in a panel stamping operation. An array of force sensors were integrated into the die structure for in-process sensing. As an introduction to this sensing method, the analytical background of the TPS surfaces is first introduced.

3.1. Thin plates spline surfaces

A TPS surface is mathematically defined as the unique function $P(x, y)$ that minimizes the bending energy function $R(P)$ in the 2D space R^2:

$$R(P) = \iint R^2 \left[\left(\frac{\partial^2 P}{\partial x^2} \right)^2 + 2 \left(\frac{\partial^2 P}{\partial xy} \right)^2 + \left(\frac{\partial^2 P}{\partial y^2} \right)^2 \right] dx\, dy \quad (4)$$

The standard solution for P that satisfies Eq. (4) is of the following form [15–17]:

$$z = P(x, y) = \sum_{j=1}^{n} a_j E(x, y) + b_0 + b_1 x + b_2 y \quad (5)$$

Here, a_j, b_0, b_1, and b_2 are constants that define a unique thin plate spline surface. The constants are calculated by applying interpolation conditions on Eq. (5). The symbol n refers to the total number of data points, and the function $E(x, y)$ is a norm defined as follows:

$$\left. \begin{array}{l} E(x, y) = J\left(\left\| (x - x_j, y - y_j) \right\| \right) \\ \|.\| = \text{length of vector} \\ \quad J(v) = v^2 \, \log(v^2) \end{array} \right\} \quad (6)$$

In Eq. (6), x_j and y_j are coordinates of the jth sensing point. Consider that there are 'n' sensors embedded in the working surface, and then the pressure measurement from each of the 'n' sensor forms an interpolation boundary condition for Eq. (5). It is important to mention that in the interpolation conditions on Eq. (5) the sensor location can only be specified in terms of two spatial coordinates (i.e. x and y). As a consequence, the spatial significance of vertical, slanting, and curved die surfaces is not incorporated into the TPS-generated surfaces, and the TPS surfaces are always defined over the outer dimensions of the sensing array.

The evaluation of the thin plate spline surfaces requires the solution of linear system equations with as many variables as there are sensors. Conventional techniques using matrix operations to solve large linear systems are time-consuming. In order to process sensor data on-line, especially for large sensor arrays, it is possible to reduce the amount of processing required by relaxing the strict interpolation requirements. This can be achieved by adding a least squares approximation term (or other similar approximation methods that are computationally less expensive) to the thin plate spline minimization function. The relaxed minimization function thus takes the form of

$$rR(P) + (1 - r)L(P) \quad (7)$$

Here, $R(P)$ is the thin plate spline minimization function and $L(P)$ is the approximation term. The symbol r represents the relaxation parameter, The least squares approximation term $L(P)$ can be expressed as

$$L(P) = \sum_{j=1}^{n} \left| P(x_j, y_j) - S_j \right|^2 \quad (8)$$

If r is 0, then the generated spline surface is a purely least squares approximation. On the other hand, if the relaxation parameter is 1, the generated surface is a strictly interpolative thin plate spline interpolation. In this study, all the TPS surfaces have been generated using strict interpolation conditions, i.e. $r = 1$.

3.2. Test-bed design and generation of TPS pressure surfaces

The design of the panel stamping setup is illustrated in Fig. 15. The test bed is designed to stamp out a 10 mm deep Aluminum panel from a $20 \times 15\,\text{cm}^2$ sheet metal of 0.51 mm thickness. The binder is mounted on four die springs, each with a spring constant of 38 N/mm to mimic the forming action of a single action stamping press. Fine adjustments to the binder force are enabled by addition of spacers to the die springs. Larger adjustments can be made by choosing springs of different stiffness. During experiments, the springs are chosen to provide a maximum of 4000 N of binder force. The clearance between the punch and die-cavity side walls is 0.60 mm. The setup was installed in a 45 kN
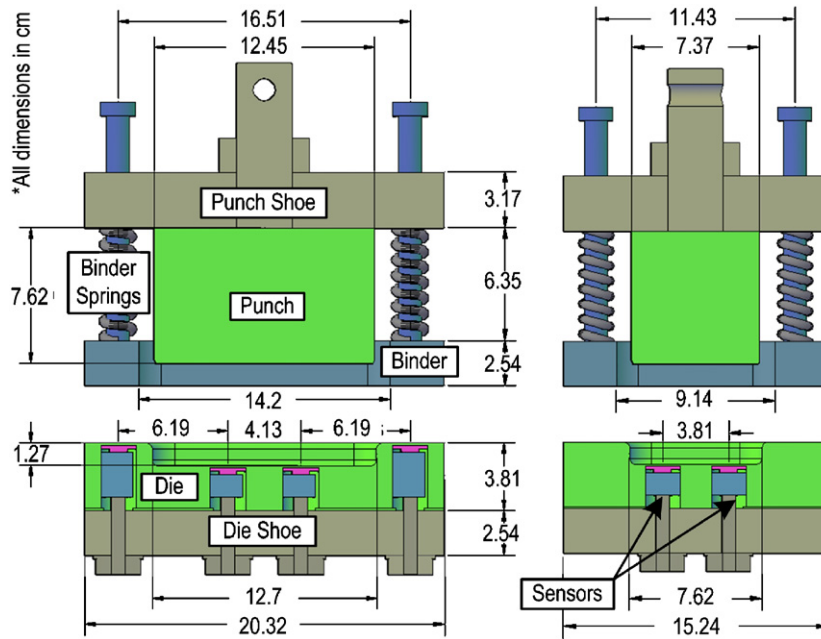
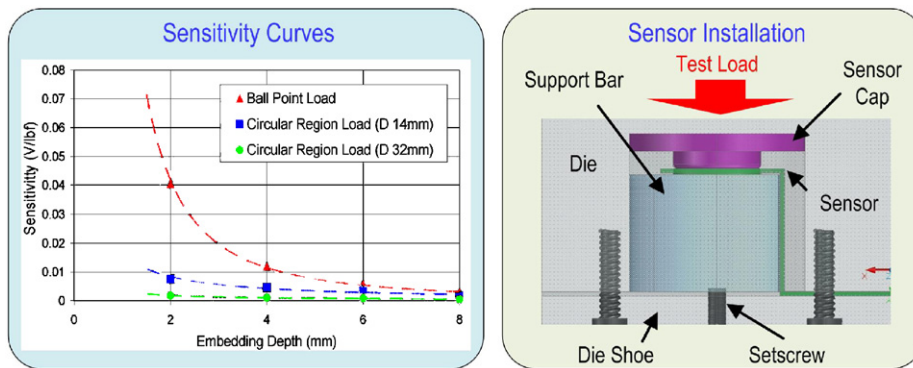**Fig. 15.** CAD drawing of experimental setup of pressure sensors.

Fig. 16. Sensitivity of embedded pressure sensors and sensor installation.

Instron hydraulic press equipped for simultaneous load and stroke monitoring.

As shown in Fig. 16, the sensitivity of the embedded sensors decreases with increased embedding depth [18]. Upon calibration, this characteristic can be utilized to provide impact protection to the sensors without compromising the measurement accuracy. To maximize sensitivity without damaging the tooling surface, the piezoresistive thin-film force sensors were embedded 1 mm under the die flange and 2 mm under the die-cavity surface (Fig. 16).

As shown in Fig. 17, 7 sensors on the die flange and 8 sensors on the die cavity were utilized for simultaneous pressure measurements during the panel stamping operation. An Instron hydraulic press was programmed to execute a sinusoidal stroke of 25 mm length with a loading and unloading time of 10 s each. In each test, the shut height was 0.6 mm.

The sensor measurements were recorded through a LabVIEW program by means of a customized signal amplification circuit and a digital data acquisition card, at a sampling rate of 100 Hz. The punch stroke and total press force was measured by sensors located within the Instron press and were sampled by the DAQ at the same sampling rate.

In Fig. 18, pressure measurements at different locations in the die cavity and on the binder (die-flange) are illustrated. The sensor numbers shown correspond to the sensor locations in Fig. 17. It is seen in Fig. 18 that the contact pressure measured by the 7 sensors on the binder or die flange increases from $T = 4$ s when the binder makes its first contact with the die flange. This trend continues until $T = 9$ s, when the trend reverses and the contact pressure starts decreasing. At $T = 15$ s, the contact pressure on the die flange starts increasing again. This observation is explained as the redistribution of the contact pressure between the die-flange and die-cavity region (see Fig. 18a for details). When the punch contacts the die-cavity surface at $T = 9$ s, it forms a rigid contact between the punch and the die. As the applied press force increases the contact pressure in the die cavity increases almost instantaneously, causing the die flange (binder) pressure to decrease. This phenomenon is an artifact of single action forming presses and it is likely that dual or multi-action forming presses would not experience the same phenomena as the binder and punch have separate actuation mechanisms. The finding is of relevance to understanding the stamping process, given the role of binder pressure in controlling the quality and geometry of a stamped product.

The TPS surfaces were calculated from the sensor measurements by a MATLAB script. Given the size difference between the die cavity and die flange, the pressure value of each surface was
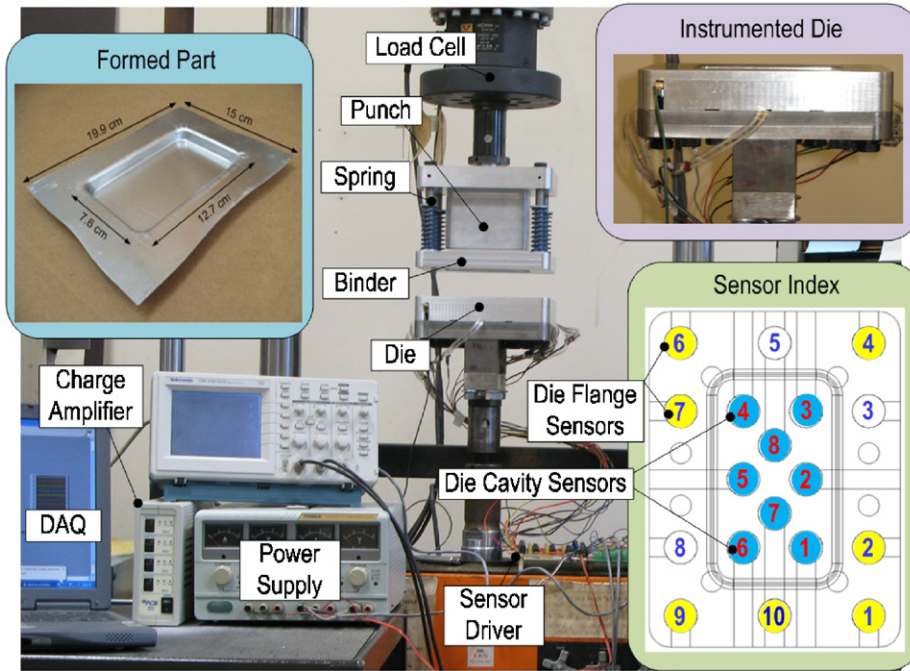
Fig. 17. Experimental bed, instrumented die, driver circuit, and sensor index of pressure sensors.
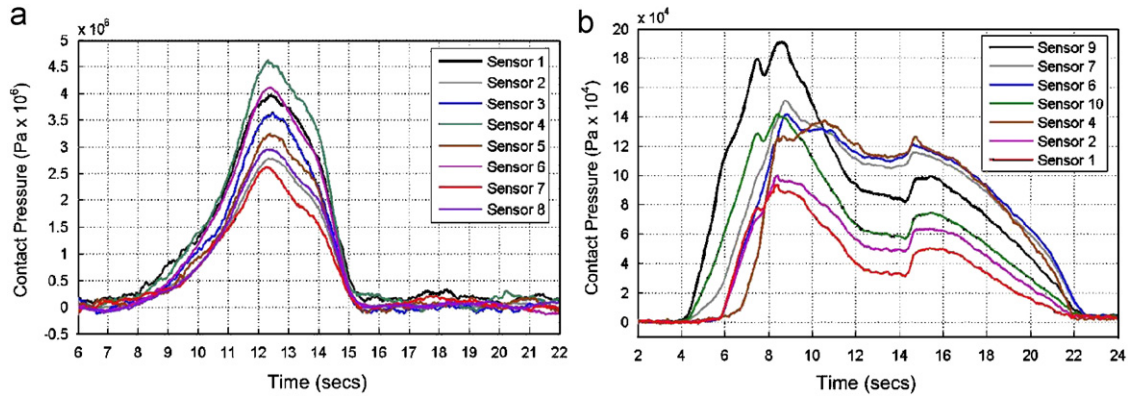

Fig. 18. Pressure measurements from sensors installed under the die surface: (A) die-cavity sensors measurements and (B) binder (die flange) sensor measurements.

calculated at 2500 grid points for the die flange and 625 grid points for the die cavity. Measurements from sensors 1, 4, 6, and 9 on the die flange were used to generate the TPS surfaces for estimating the contact pressure on the die flange, as illustrated in Fig. 19. Fig. 20 illustrates the TPS-estimated contact pressure on the die cavity using sensors 1–8 installed under the cavity, where each surface is indexed against the press force and punch stroke at that instant. The table inset provides the average pressure calculated from the die-cavity pressure surfaces. Each distinct surface represents the TPS-calculated estimate of the pressure distribution at a time instant. For visual clarity, only 10 and 8 surfaces are shown here, corresponding to the pressure distribution on the die flange and die cavity, respectively. It is noted from the TPS surfaces that the contact pressure distribution on the die-flange and die-cavity surfaces has unsymmetrical features, even though the product and tooling geometry is symmetrical. This is attributed to the fact that the fixture structure for the die and punch assemblies has an inherent mechanical compliance. The
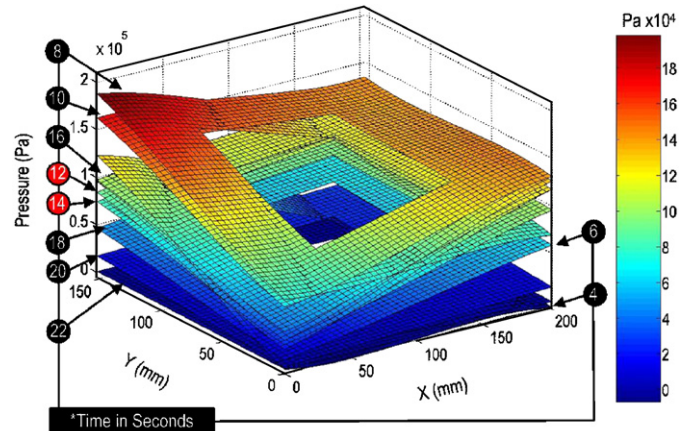

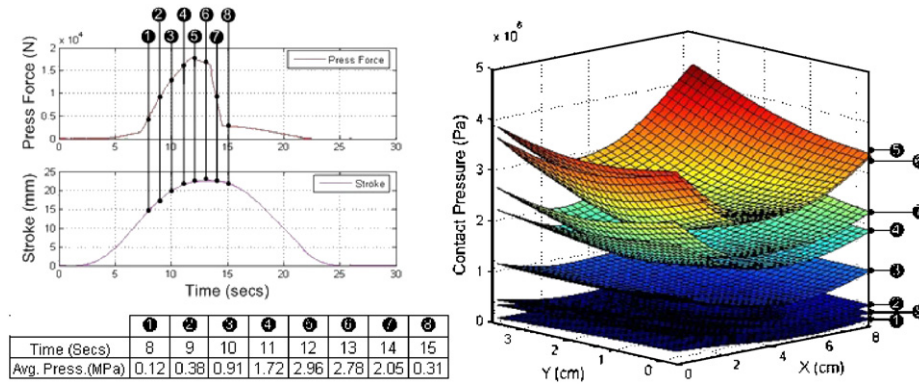Fig. 19. TPS surfaces evaluated from force sensors embedded in die flange.

Fig. 20. TPS surfaces evaluated from force sensors embedded in die cavity.

mechanical compliance is not constant; it can vary with press speed, workpiece positioning, and gradual variations, caused by tool wear. The embedded sensors thus provide a method for quantifying the otherwise unpredictable variations in the stamping process.

The TPS surfaces corresponding to the die flange (Fig. 19) reflect the decrease in pressure noted in the sensor measurements and attributed to the redistribution of force between the binder and the die cavity. Specifically, TPS surfaces at $T = 8$ and $16\,s$ display higher contact pressure in comparison to surfaces at $T = 12$ or $14\,s$. This effect is most prominent on the far left corner of the surfaces (location $X = 0\,mm$, $Y = 150\,mm$). Upon evaluation of the TPS interpolating surfaces from discrete sensor measurements, the accuracy of the method in estimating the contact pressure in regions where there are no sensors can be estimated. This is demonstrated in the following section.

3.3. Accuracy of TPS-based estimation

The accuracy of TPS surfaces in estimating the contact pressure on the tool–workpiece surface has been evaluated by two methods: (a) through comparison between the TPS interpolated die-flange (binder) pressure and measurements from sensors 2, 7, and 10, which were not included in the surface generation calculations, and (b) through comparison between the binder and punch force calculated from numerical integration of the TPS surfaces against the measured press force. The result of comparison between estimated and actual pressure at the sensor locations 2, 7, and 10 is shown in Fig. 21. The average relative error between the actual and estimated pressure at sensor locations 2, 7, and 10 is less than 5%, 3%, and 7%, respectively. In the second method where force, instead of pressure, is compared, to determine the net force acting on the working interface, the TPS-estimated pressures were numerically integrated over the die-cavity and die-flange surface area, based on the following equation:

$$^{Int}F_{Surface}(t) = \sum_{i=1}^{n} \sum_{j=1}^{m} P_{i,j}(t)\, dA(i,j) \tag{9}$$

Here, $^{Int}F_{Surface}(t)$ is the surface integrated die-flange (binder) or die-cavity (punch) force at time t. The constants n and m represent the number of divisions into which the contact surface is partitioned for numeric integration. The term $dA(i, j)$ is the area of the surface element at location (i, j) on the contact surface, and $P_{i,j}(t)$ is the pressure acting on that area element at time t. For the calculation of contact force from experimental measurements, the value of n and m was taken to be 50. Fig. 22 shows the surface integrated binder force, the sum of the surface integrated binder
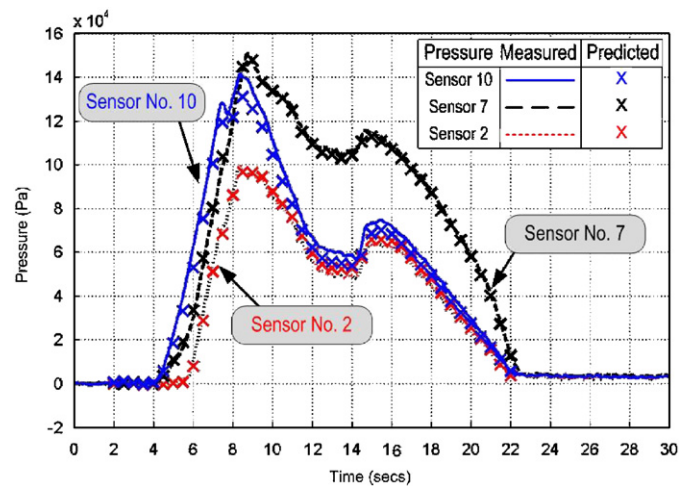

Fig. 21. Comparison of TPS estimated and actual pressure at sensor locations 2 and 7.
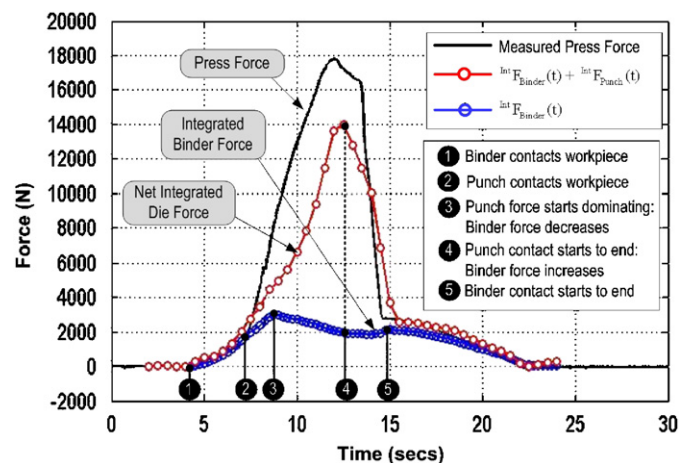

Fig. 22. Comparison of press force, die spring force, and surface integrated binder force.

and punch force, and the load cell measured press force. Neglecting the side wall friction and contact surfaces not included in the sensor coverage, the press force measured by the load cell should be related with the sum of the contact force exerted on the die flange (binder) and die cavity (punch force). The trend of the $^{Int}F_{Binder}(t)$ and that of the measured force agrees well with each

other (over 96%), in the time interval before and after the punch is in contact with the workpiece. The net integrated force (sum of integrated punch and binder force) is found to be in less agreement with the load cell measured press force, with an error of 22% at peak press force. This error is attributed to the fact that the sensing scheme does not account for frictional forces acting on the side walls of the die cavity. In addition, the edges of the die cavities are known to have large contact stresses [19] not accounted for, due to the structural difficulty in integrating sensors into the edges. This problem can be addressed by using miniaturized sensor packages for structural integration into the die edges. Based on the experimental results, it can be concluded that TPS-based interpolation is a robust and accurate method for creation of continuous contact pressure profiles from spatially discrete sensor measurements.

4. Conclusions

Real-time monitoring of local draw-in amount and local contact pressure in a deep drawing process is highly desirable for effective process control and for the time reduction needed for die trial out. Two tooling-integrated sensing methods were quantitatively evaluated using experimental setups. The non-contact draw-in sensor embedded in binders is based on the law of mutual inductance demonstrating excellent repeatability. It provided a nearly linear output characteristic between the sheet displacement and the output voltages, and was shown to be insensitive to the form of the sheet material when the sheet thickness is less than 1 mm, i.e. flat or wrinkled sheet provided the same reading, which is highly desired in this application. The functionality of the draw-in sensors was verified by integrating them into an industry-scale setup. The die cavity and die flange in a panel stamping test-bed was embedded with thin-film force sensors to measure the tool–workpiece contact pressure at multiple locations. Thin plate spline surfaces were studied to evaluate spatially continuous pressure profiles from the discrete measurements. The net binder force estimated by integration of binder pressure over the contact region was found to have an error of less than 4%. It was further determined through redundant sensor sites that the contact pressure at random locations on the binder can be estimated with an accuracy of better than 93%. An integrated sensing system incorporating both the draw-in and pressure sensors into a single tool structure is currently being designed. Such a system can be used for process diagnosis, process optimization and/or process control to increase the efficiency of material utilization in sheet metal forming.

References

[1] K. Siegert, E. Dannenmann, S. Wagner, A. Galaiko, Closed-loop control system for blank holder forces in deep drawing, CIRP Annals 44 (1) (1995) 251–254.
[2] T. Buranathiti, J. Cao, Benchmark analysis on forming of an automotive deck lid inner panel, in: NumiSheet 2005 Conference Proceedings, Detroit, MI, 2005.
[3] K. Siegert, Institute of Metal Forming Technology, Stuttgart University, Germany.
[4] S.K. Kernosky, K.J. Weinmann, J.R. Michler, A.R. Kashani, Development of a die shoulder force transducer for sheet metal forming research, Journal of Manufacturing Science and Engineering 120 (1988) 42–48.
[5] J. Cao, X. Wang, An analytical prediction of flange wrinkling in sheet metal forming, Journal of Manufacturing Processes 2 (2) (2000) 100–107.
[6] Z.Q. Sheng, S. Jirathearanat, T. Altan, Adaptive FEM simulation for prediction of variable blank holder force in conical cup drawing, International Journal of Machine Tools and Manufacture 44 (5) (2004) 487–494.
[7] S.K. Kernosky, K.J. Weinmann, J.R. Michler, A.R. Kashani, Development of a die shoulder force transducer for sheet metal forming research, Journal of Manufacturing Science and Engineering—Transactions of the ASME 120 (1998) 42–48.
[8] H. Du, B.E. Klamecki, Force sensors embedded in surfaces for manufacturing and other tribological process monitoring, Journal of Manufacturing Science and Engineering—Transactions of the ASME 121 (4) (1999) 739–748.
[9] M. Li, B.E. Klamecki, K.J. Weinmann, SN-gage and instrumented pin: to measure shear and normal tool forces in sheet metal forming, Transactions of North American Manufacturing Research Institution/Society of Manufacturing Engineers 20 (1992) 103–109.
[10] M.C. Doolan, S. Kalyanasundaram, P. Hodgson, M.J. Cardew-Hall, Identifying variation in sheet metal, Journal of Materials Processing Technology 115 (2001) 142–146.
[11] J. Breitling, D. Wallace, T. Altan, Investigations of different loading conditions in a high speed mechanical press, Journal of Materials Processing Technology 59 (1996) 18–23.
[12] W. Klingenberg, T.W. de Boer, Condition based maintenance in punching/blanking of sheet metal, International Journal of Machine Tools and Manufacture 48 (5) (2008) 589–598.
[13] P. Kopczynski, LVDTs. Theory and application, Sensors 9 (1992) 18–22.
[14] D.-J. Choi, C.-T. Rim, et al., High sensitivity inductive sensing system for position measurement, IEEE Instrumentation and Measurement Technology Conference 2 (2000) 595–599.
[15] G. Wahba, Spline Models for Observational Data, Capital City Press, 1992.
[16] F.L. Bookstein, Principal warps: thin plate splines and the decomposition of deformations, IEEE Transactions on Pattern Analysis and Machine Intelligence 11 (1989) 567–585.
[17] J. Duchon, Interpolation des fonctions de dux variables suivant le principe de la flexion des plaques minces, RAIRO Analyse Numérique 10 (1976) 5–12.
[18] J. Hanchi, M. Li, B.E. Klamecki, Sensing of interface loads in manufacturing processes, Tribological Aspects in Manufacturing, American Society of Mechanical Engineers 2 (1991) 203–216.
[19] M. Oudjene, J.-L. Batoz, L. Penazzi, F. Mercier, A methodology for the 3D stress analysis and the design of layered sheet metal forming tools joined by screws, Journal of Materials Processing Technology 189 (2007) 334–343.